Torque Generated by the Flagellar Motor of *Escherichia coli* while Driven Backward

Richard M. Berry and Howard C. Berg

Department of Molecular and Cellular Biology, Harvard University, Cambridge, Massachusetts 02138 and Rowland Institute for Science, Cambridge, Massachusetts 02142

ABSTRACT   The technique of electrorotation was used to apply torque to cells of the bacterium *Escherichia coli* tethered to glass coverslips by single flagella. Cells were made to rotate backward, that is, in the direction opposite to the rotation driven by the flagellar motor itself. The torque generated by the motor under these conditions was estimated using an analysis that explicitly considers the angular dependence of both the viscous drag coefficient of the cell and the torque produced by electrorotation. Motor torque varied approximately linearly with speed up to over 100 Hz in either direction, placing constraints on mechanisms for torque generation in which rates of proton transfer for backward rotation are limiting. These results, interpreted in the context of a simple three-state kinetic model, suggest that the rate-limiting step in the torque-generating cycle is a powerstroke in which motor rotation and dissipation of the energy available from proton transit occur synchronously.

INTRODUCTION

The bacterial flagellar motor is a rotary molecular engine driven by ions moving inwards across the cytoplasmic membrane (Macnab, 1996). Each motor turns an external helical filament, which generates the thrust enabling cells to swim. The ion flux is powered by an electrochemical gradient, either a protonmotive force (pmf) or sodium-motive force (Namf), in motors driven by H^+ or Na^+, respectively. Filaments rotate at a few hundred Hz in cells driven by H^+ motors (Lowe et al., 1987) and up to 1000 Hz in cells driven by Na^+ motors (Magariyama et al., 1994). If cells are attached ("tethered") to a surface by a single flagellar filament, the motor turns the cell body alternately clockwise (CW) and counterclockwise (CCW) at speeds around 10 Hz (Silverman and Simon, 1974). The switching between these modes is stochastic (Khan and Macnab, 1980; Scharf et al., 1998). Control of the direction of rotation provides the basis for bacterial chemotaxis (Larsen et al., 1974).

Models proposed for the mechanism of torque generation in the flagellar motor make different predictions for the relationship between torque and speed. In particular, in models in which ion flux is strictly proportional to rotation rate and rates for proton transfer for backward rotation are limiting, torque will rise sharply if the motor is driven backward beyond some limiting speed. Barriers of this kind were predicted for a thermal ratchet model by Meister et al. (1989) and observed (or so it was thought at the time) by Berg and Turner (1993) in experiments in which torque was applied to tethered cells by high-frequency rotating electric fields (Washizu et al., 1993). Closer analysis suggested that these barriers were an artifact due to ellipticity in the electric field (Berry and Berg, 1996). This was confirmed using optical tweezers: the motor generated the same torque when made to rotate slowly backward as when allowed to rotate slowly forwards at speeds up to 0.3 Hz (Berry and Berg, 1997). In the present work, we return to the electrorotation experiments and show, by analyzing separately data obtained at different angles of the cell body, that there is no barrier to backward rotation at speeds up to 40 Hz. Data obtained from one particular cell that showed unusually low angular variation in the torque generated by electrorotation indicate that the linear range of the torque-versus-speed relationship extends up to > 100 Hz in either direction. These results are interpreted in the framework of a simple kinetic model.

MATERIALS AND METHODS

Cell strains, their growth and tethering, electrorotation, and data acquisition were as described previously (Berg and Turner, 1993).

RESULTS

In an electrorotation experiment, one varies the amplitude and sign of the externally applied torque by varying the amplitude and direction of rotation of a high-frequency rotating electric field. The amplitude of the applied torque is proportional to the square of the electric field. We refer to this amplitude as electrorotation strength, P, and report it as a percentage of the maximum possible with the apparatus that we used. Fig. 1 shows the speed of rotation of a tethered cell of *E. coli* strain KAF95 (Fahrner, 1995) as a function of electrorotation strength. When spinning on its own, such a cell rotates exclusively CCW. The solid line shows the cell speed averaged over successive periods of 1/6 s during a run
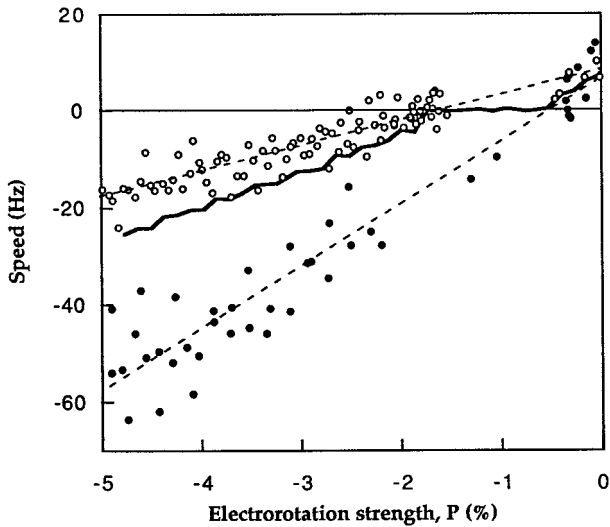
FIGURE 1 Speed of rotation of a tethered cell of *E. coli* strain KAF95 (motor torque CCW) as a function of the electrorotation strength. The solid line shows the cell speed averaged over successive periods of 1/6 s, during a run in which the applied torque was steadily increased from 0 to −5%. The filled and open circles show the speeds during the same run while the angle of the cell body was in the ranges 120° to 180° and 240° to 300°, respectively. The dashed lines are fits to these data by linear regression.
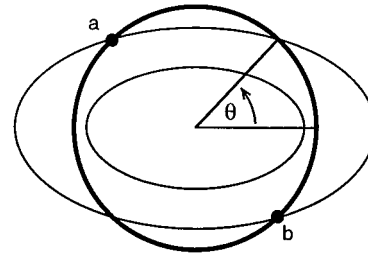

FIGURE 2 The amplitude of the torque exerted on the body of a tethered cell by its flagellar motor (*thick curve*) or by an externally applied high-frequency rotating electric field (at small or intermediate amplitudes, *thin curves*) shown as a function of the angular position of the cell, θ. The body of the cell spins at a speed proportional to the sum of these two torques, i.e., at a speed proportional to the sum of the radii of the circle and the ellipse at any given angle. It is assumed that the motor drives the cell CCW, in the direction of increasing angle. If the externally applied torque opposes this motion and has a strength shown by the larger ellipse, the cell stops at a or b.

in which P was steadily increased from 0 to −5%. These data were previously interpreted as a barrier to backward rotation of the flagellar motor (Berg and Turner, 1993), as they appear to indicate that almost twice as much torque is required to make the motor rotate backward as is sufficient to stop its rotating forwards. However, separation of the data into subsets according to the angle of the cell body shows that at each angle the relationship between speed and applied torque is actually linear. Evidently, the externally applied torque was larger when the cell was oriented between 120° and 180° (*filled circles, steeper slope*) than it was when it was oriented between 240° and 300° (*open circles*). Gaps appear in the records shown by the circles, because at these values of electrorotation strength the motor was stalled with the cell body at angles different from those included in the figure.

The apparent barrier to backward rotation (Fig. 1, *solid line*) appears because the electrorotation strength required to stall the motor varies with cell angle (Berry and Berg, 1996). This is shown schematically in Fig. 2, where the motor torque, assumed independent of angle, appears as a circle, while the externally applied torque (at small or intermediate strength) appears as an ellipse. If the externally applied torque augments motor torque, then the cell speeds up. If the externally applied torque opposes motor torque, then the cell slows down. Its speed is proportional to the algebraic sum of the radii of the circle and the ellipse, and this varies with angle. When the externally applied torque opposes motor torque and its strength is sufficiently large, the cell stops or turns backward. For a strength corresponding to the larger ellipse in Fig. 2, the cell stops at *a* or *b*, where motor torque and externally applied torque balance.

The cell rotates continuously backward only at larger strengths, when the minor radius of the ellipse is larger than the radius of the circle.

We can obtain an estimate of the torque-speed relationship of the motor that is unaffected by the angular variation in electrorotation strength by considering each angle separately. At a given angle of the cell body, θ, the following balance of torques applies:

$$f_\theta \omega = a_\theta P + T(\omega) \tag{1}$$

where P is the electrorotation strength, $T(\omega)$ is the torque generated by the motor at speed ω, and both the frictional drag coefficient of the cell body, f_θ, and the torque generated for a given electrorotation strength, a_θ, are functions of θ (Berry and Berg, 1996). With $P = 0$, the cell speed at a given angle, ω_θ^o, gives for the drag coefficient at that angle

$$f_\theta = T(\omega_\theta^o)/\omega_\theta^o. \tag{2}$$

The constant of proportionality between electrorotation strength and torque is given by the electrorotation strength required to stall the motor, P_θ^s, via

$$a_\theta = -T(0)/P_\theta^s. \tag{3}$$

After substitution of Eqs. 2 and 3 into Eq. 1, and assuming f_θ and a_θ are independent of speed, we obtain the following expression for the relative torque generated by the motor at speed ω:

$$\frac{T(\omega)}{T(\omega_\theta^o)} = \frac{\omega}{\omega_\theta^o} + \frac{T(0)}{T(\omega_\theta^o)}\frac{P}{P_\theta^s}. \tag{4}$$

Data were separated into 6 bins each containing all points (P_i, ω_i) for which the cell angle fell into a particular 60 degree range. Values of ω_θ^o were obtained for each bin by averaging the speeds measured in the absence of electrorotation, and values of P_θ^s were taken as the zero-speed intercept in line fits of ω_i versus P_i for each angle, constrained to

pass through the point $(0, \omega_\theta^o)$. The relative torque was then calculated for each point via Eq. 4, and data from all angles were pooled and averaged. The unknown parameter in Eq. 4, $k = T(0)/T(\omega_\theta^o)$, was set to 1, which assumes that the torque generated by a motor in a freely spinning tethered cell is equal to the stall torque. The validity and consequences of this assumption are considered in the discussion.

Fig. 3 *a* shows calculated values of relative torque as a function of speed for the cell of Fig. 1. The points close to zero torque were obtained after a catastrophic break (Berg and Turner, 1993) when the cell did not rotate on its own and its speed was directly proportional to the applied torque. The data obtained before the motor was broken indicate that the motor torque is constant. If k is not actually equal to 1, the data indicate, instead, that motor torque varies linearly with speed. Figure 3 *b* shows the results of a similar analysis for another cell, whose motor remained intact. As in Fig. 3 *a*, the torque varies linearly with speed or, if the assumption $k = 1$ holds, is constant.

The data in Fig. 1 show that the torque-speed relationship is linear between $+20$ and -40 Hz. Cells which were made

to rotate considerably faster than this also showed approximately linear variation of speed with applied torque at each angle, as in Fig. 3 *a*. However, the quality of data obtained from these cells was insufficient for the analysis leading to Fig. 3, *a* and *b*. One reason for this was that at higher speeds, experimental noise and the data sampling frequency of 1 kHz led to insufficient resolution of cell speed at different angles within a single revolution. Another reason was that the orientation of the tether and therefore the drag coefficient of the cell body appeared to change as cells were made to rotate backward at high speeds. This appeared as differences in the shapes of the speed-versus-applied torque curves for different angles, with a greater than linear increase of speed with torque at some, but not all, angles.

In order to examine the torque-speed relationship of the flagellar motor when driven backward at speeds greater than 40 Hz we reverted to a simpler analysis of one particular cell that appeared, fortuitously, to show very little angular variation in the torque generated by electrorotation, and as a consequence did not require the more complicated analysis described above. Fig. 4 shows data taken using electrorotation on a cell of the strain KAF84 (Fahrner, 1995) in which the motor switches direction. This cell was remarkable in that the motor did not show an apparent barrier to backward rotation, and also in that it was not completely broken even after being made to rotate backward several times at over 100 Hz. Fig. 4 *a* shows the speed of rotation, averaged over all angles, as a function of electrorotation strength. Torque was applied repeatedly over various ranges between -5 and $+5\%$ while the motor switched randomly between directional modes; data from several runs are plotted together in the figure. Data points fall approximately on two parallel lines, one for each directional mode of the motor, symmetrically disposed about the origin and separated by about 20 Hz, twice the unassisted rotation rate. Fig. 4 *b* shows relative torque versus speed for this cell, calculated according to Eq. 4, with $\omega^o = 12$ Hz and $P^s = -0.45\%$ replacing ω_θ^o and P_θ^s, respectively. Similarly to the data of Fig. 1, torque varies linearly with speed between $+40$ and -30 Hz in the CCW or positive directional mode. The step down in torque above $+40$ Hz appears because the motor was partially broken (presumably while it was driven backward; Berg and Turner, 1993) before being made to rotate faster than $+40$ Hz. The upward turn in relative torque in both modes at negative speeds beyond -50 Hz may be a genuine feature of the motor, but we believe that it is more likely to reflect an increase in the viscous drag coefficient of the cell body at these speeds. If f_θ increased or a_θ decreased with speed, the change in speed due to electrorotation would be less than if f_θ and a_θ were constant, and Eq. 4 would overestimate the motor torque at high negative speeds. We conclude that the torque-speed relationship of the flagellar motor is approximately linear at speeds up to at least 100 Hz in either direction in the CCW mode, and at speeds up to at least 130 Hz forwards (in the same direction as motor torque) in the CW mode.
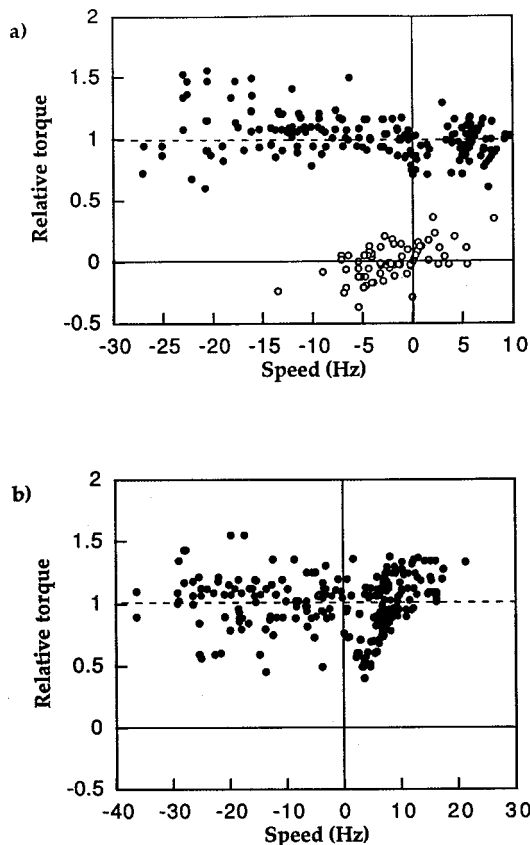

FIGURE 3   (*a*) Relative torque generated by the motor as a function of motor speed during the run depicted in Fig. 1 and subsequent similar runs. The filled and open circles were obtained before or after the flagellar motor of this cell was broken, respectively. The dashed line indicates relative torque 1. (*b*) Relative torque versus speed, as in Fig. 3 *a*, but for a different cell. The flagellar motor of this cell was not broken. The dashed line indicates relative torque 1.

a)

b)

FIGURE 5　A simple kinetic model for the mechanochemical cycle of torque-generating units in the bacterial flagellar motor. The cycle is reduced to three steps. Steps 1 and 3 involve exchange of protons between the motor and the periplasm or cytoplasm respectively, while step 2 incorporates all events that occur while protons are within the motor. Rate constants for steps leading to forwards and backward cycles are labeled k_{fi} and k_{bi} respectively, where i indicates the step.
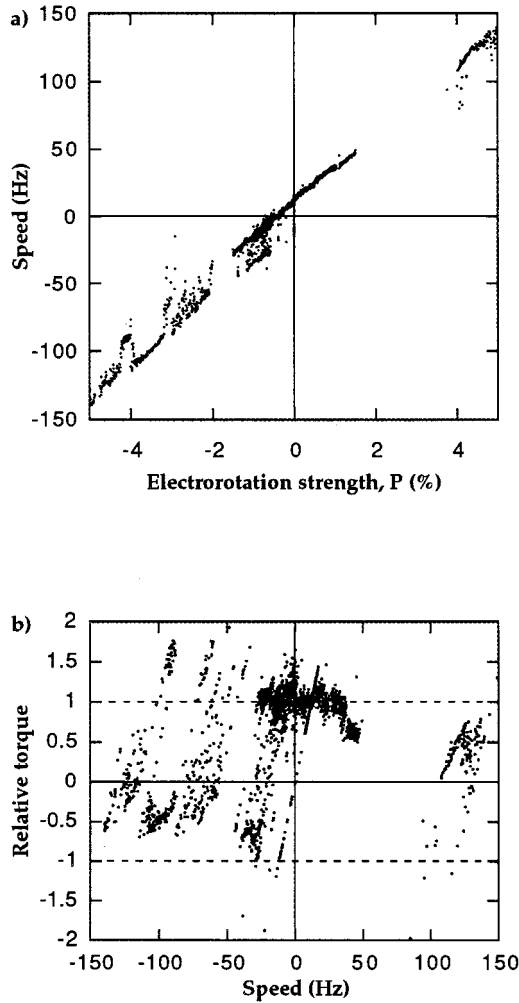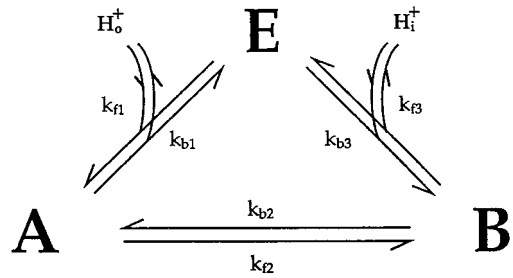
FIGURE 4　(*a*) Speed of rotation of a tethered cell of *E. coli* strain KAF84 (wild-type for chemotaxis) as a function of the electrorotation strength. Electrorotation strength was varied over several ranges between -5 and $+5\%$ during 10 separate runs, while the motor switched spontaneously between directional modes. Data from all runs are plotted together in the figure. Data points fall close to two parallel lines, one for each directional mode of the motor. (*b*) The same data as in Fig. 4 *a*, plotted as relative torque generated by the motor as a function of motor speed. The dashed lines indicate relative torques 1, -1.

DISCUSSION

The torque-speed relationship in the bacterial flagellar motor is linear at speeds up to 100 Hz in either direction. This allows us to rule out those models of the mechanism of flagellar rotation that predict a barrier to backward rotation. Barriers to backward rotation are predicted by models where rotation is tightly coupled to the flux of ions through the motor and where the rate of transit of ions against their electrochemical gradient is strictly limited (Läuger, 1988; Meister et al., 1989). At a kinetic rather than mechanical level, the torque-speed curve can be understood in terms of the torque dependence of the rate-limiting step in the torque-generating cycle. This can be illustrated by a simple kinetic model. Fig. 5 shows a minimal kinetic scheme for

the mechanochemical cycle of a torque-generating unit in the flagellar motor. The unit moves between state E and states A or B (steps 1 and 3, respectively) by exchange of protons with either the cytoplasm (H_i) or the periplasm (H_o), and any processes that occur while a proton is within the motor are summarized by the transition between states A and B (step 2). We shall assume tight coupling between proton flux and rotation. Thus we can specify the torque against which the motor is acting and determine the corresponding proton flux and speed from the net rate at which the kinetic cycle $E \rightarrow A \rightarrow B \rightarrow E$ is performed.

Each step, i, in the cycle can, in general, involve a chemical free energy change, U_i, and simultaneously the rotation of the rotor through some angle, ϕ_i. In such a step, the unit performs work $W_i = \Gamma\phi_i = \beta_i\Gamma\phi$, where Γ is the torque, ϕ is the angle moved in one cycle, and β_i is the fraction of that distance moved in step i. The sum of all U_i over one cycle must be equal to $ne\Delta p$, the electrochemical potential energy available from the translocation across the membrane of n protons, each with charge e, driven by a pmf Δp. If we let $U_i = \alpha_i ne\Delta p$, the parameters α_i are a measure of the fraction of the available free energy of protons dissipated in each step. Here we use the term "dissipated" to denote the conversion of chemical energy into either heat or work. In a physically explicit model the electrochemical energy of protons is converted to work via some intermediate form, usually electrostatic energy or the conformational energy of stretching a molecular spring. This level of detail is not included in our simple kinetic model, and the conversion of free energy between such intermediate forms is not considered explicitly.

Regardless of the nature of the step, i, the ratio of its forwards to backward rates will vary as $\exp[(U_i - W_i)/kT]$, where k is Boltzmann's constant and T the absolute temperature (Klein and Meijer, 1954). For instance, as the torque increases either the forwards rate must decrease or the backward rate must increase for any transition where ϕ_i is positive. The larger the angle, ϕ_i, the greater the change. Similarly, any step that involves the transit of protons through a significant portion of Δp will be biased in the

forwards direction. The absolute rates of these transitions and the distribution of the effects of Γ and Δp between forwards and backward rates will depend upon the physical details of the model.

For the sake of simplicity, we assume that forwards and backward rates are affected symmetrically, and the rate constants for step i are given by

$$k_{fi} = k_i \exp\left(\frac{U_i - W_i}{2kT}\right) \tag{5}$$

$$k_{bi} = k_i \exp\left(\frac{-U_i + W_i}{2kT}\right), \tag{6}$$

where k_i are constants that determine the absolute speed of each step. Numerical solution of the equations

$$\frac{dP_E}{dt} = k_{b1} \cdot P_A + k_{f3} \cdot P_B - (k_{f1} + k_{b3}) \cdot P_E = 0 \tag{7}$$

$$\frac{dP_A}{dt} = k_{b2} \cdot P_B + k_{f1} \cdot P_E - (k_{f2} + k_{b1}) \cdot P_A = 0 \tag{8}$$

$$\frac{dP_B}{dt} = k_{b3} \cdot P_E + k_{f2} \cdot P_A - (k_{f3} + k_{b2}) \cdot P_B = 0 \tag{9}$$

gives the steady-state occupancy probabilities, P_E, P_A, and P_B, of the different motor states. From these we obtain the net rate of the mechanochemical cycle as

$$f = k_{f2} \cdot P_A - k_{b2} \cdot P_B. \tag{10}$$

The rotation rate is given by $\omega = f\phi$ because we have assumed tight coupling.

With a pmf of 150 mV and a temperature of 300 K, we have $e\Delta p = 24$ pN.nm $= 6kT$. The distance moved in one cycle, ϕ, is unknown, but we can make educated guesses. Each torque-generating unit completes $n_s = 2\pi/\phi$ cycles per revolution of the rotor. If each cycle involves the transit of one proton and there are n_u units, then one revolution will be coupled to the transit of $n_s n_u$ protons across the membrane. The torque is equal to the work done in one revolution divided by 2π radians, and the work done must be less than or equal to $24 n_s n_u$ pN.nm. Therefore, the torque must be less than $24/2\pi$ $n_s n_u$ pN.nm/radian, or $3.8 n_s n_u$ pN.nm. The stall torque has been measured to be in the vicinity of 4000 pN.nm (Berry and Berg, 1997) and the proton flux is thought to be around 1000 per revolution (Meister et al., 1987), confirming that the motor operates close to unit efficiency at stall. It is not absolutely clear how many torque generators there are in a normal flagellar motor. With $n_s n_u = 1000$ and $n_u = 8$ units per motor, we have $n_s = 125$, while if $n_u = 16$ then $n_s = 62$. The flagellar rotor has an axial symmetry of about 30 (Jones et al., 1990; Sosinsky et al., 1992), and it seems reasonable to expect n_s to be some multiple of this number. Fluctuation analysis has suggested that each unit takes at least 50 steps per revolution (Samuel and Berg, 1996). Taking all these factors into consideration, we shall assume that $n_u = 8$ and $n_s = 120$ in our simulations

when one proton is translocated per cycle. It should be stressed, however, that the predictions of the model do not depend critically upon these numbers. For instance, if we chose $n_u = 16$ and $n_s = 60$ and halved the rate constants, k_i, the torque generated per unit would be halved, the number of cycles per second (each cycle moving the rotor twice the distance) would be halved, and the predicted torque-speed relationship for the entire motor would be unchanged.

The left-hand panels in Fig. 6 show torque-versus-speed relationships predicted by the model for flagellar motors with different values of the parameters α_i and β_i, which are represented graphically in the corresponding right-hand panels. We have assumed that the torque generated by the entire motor at any given speed is simply n_u times the torque generated by a single unit at the same speed. This has been shown at low speeds from "resurrection" experiments in which wild-type torque-generating units were expressed in tethered cells of paralyzed mutants (Block and Berg, 1984; Blair and Berg, 1988) and at higher speeds in similar experiments in which flagellar filament stubs were marked with small latex beads (Ryu, W., R.M. Berry, and H.C. Berg, manuscript in preparation).

In Fig. 6 *a*, all α_i and β_i are equal to 1/3, and the predicted torque-speed curve is approximately linear at speeds up to several hundred Hz in either direction. Fig. 6 *b* shows the case where protons are passed through the membrane in step $E \to A$ to a torque-generating apparatus at the cytoplasmic side. This represents a thermal ratchet mechanism in that the step that generates motion is not directly driven by the dissipation of a significant fraction of the free energy that powers the motor. Rather, this free energy serves to bias the forwards reaction indirectly, in this case by increasing the probability of state *A* via the transit of protons across the membrane. The left-hand panel of Fig. 6 *b* shows the barrier to backward rotation that is predicted for a mechanism of this type. Such a barrier will exist if there is any step in the cycle that dissipates the free energy of protons without rotation. The reverse rate of this step will be relatively slow, due to large U_i, and will remain slow even in the face of greatly increased torque, due to small W_i. Even very large torques will not cause a significant speeding up of the backward flow of ions, and if the tight-coupling assumption holds, this means a corresponding limit to the rate of backward rotation. A barrier of this kind is predicted by the tight-coupled model of Meister et al. (1989). It is observed experimentally in the ATP-powered linear kinesin/microtubule motor of eukaryotes (Coppin et al., 1997), probably indicating tight coupling between translation of the motor and an essentially irreversible step involving ATP hydrolysis.

For a tight-coupled model to predict constant torque at speeds up to at least 100 Hz in either direction, in line with experimental results using electrorotation (Berg and Turner, 1993), there must be a rate-limiting step in the torque-generating cycle with a rate that is extremely sensitive to torque. This is illustrated in Fig. 6 *c* where step 2 in the model contains most of the motion that occurs during a cycle and also dissipates most of the available free energy of

FIGURE 6 The relationship between torque and speed predicted by the model of Fig. 5 (*left-hand panels*) with different sets of parameters as described in the text. The right-hand panels are a graphic representation of the degree to which each step in the mechanochemical cycle dissipates the free energy available from proton translocation (*vertical axes*) and results in rotation of the rotor (*horizontal axes*). (*a*) With all three steps equivalent, the predicted torque-speed relationship is approximately linear up to several hundred Hz in either direction. Parameters: $\alpha_1 = \alpha_2 = \alpha_3 = \beta_1 = \beta_2 = \beta_3 = 1/3$, $k_1 = k_2 = k_3 = 6 \times 10^4 \text{ s}^{-1}$. (*b*) If the dissipation of proton free energy and the rotation of the rotor occur in separate steps, the model predicts a barrier to backward rotation. Parameters: $\alpha_1 = \beta_2 = 0.95$, $\alpha_2 = \alpha_3 = \beta_1 = \beta_3 = 0.025$, $k_1 = k_2 = k_3 = 10^5 \text{ s}^{-1}$. (*c*) If a single step couples proton free energy to rotation, the predicted torque-speed relationship shows a region of slowly varying torque (a plateau) at low speeds, and a steeper torque dependence at higher speeds. The plateau is made flatter by increasing both the distance moved and the number of protons translocated in each cycle (*open circles*). Parameters: $\alpha_2 = \beta_2 = 0.95$, $\alpha_1 = \alpha_3 = \beta_1 = \beta_3 = 0.025$, $k_1 = k_2 = k_3 = 10^5 \text{ s}^{-1}$ (*closed circles*); $k_1 = k_2 = k_3 = 4.2 \times 10^4 \text{ s}^{-1}$ (*open circles*).
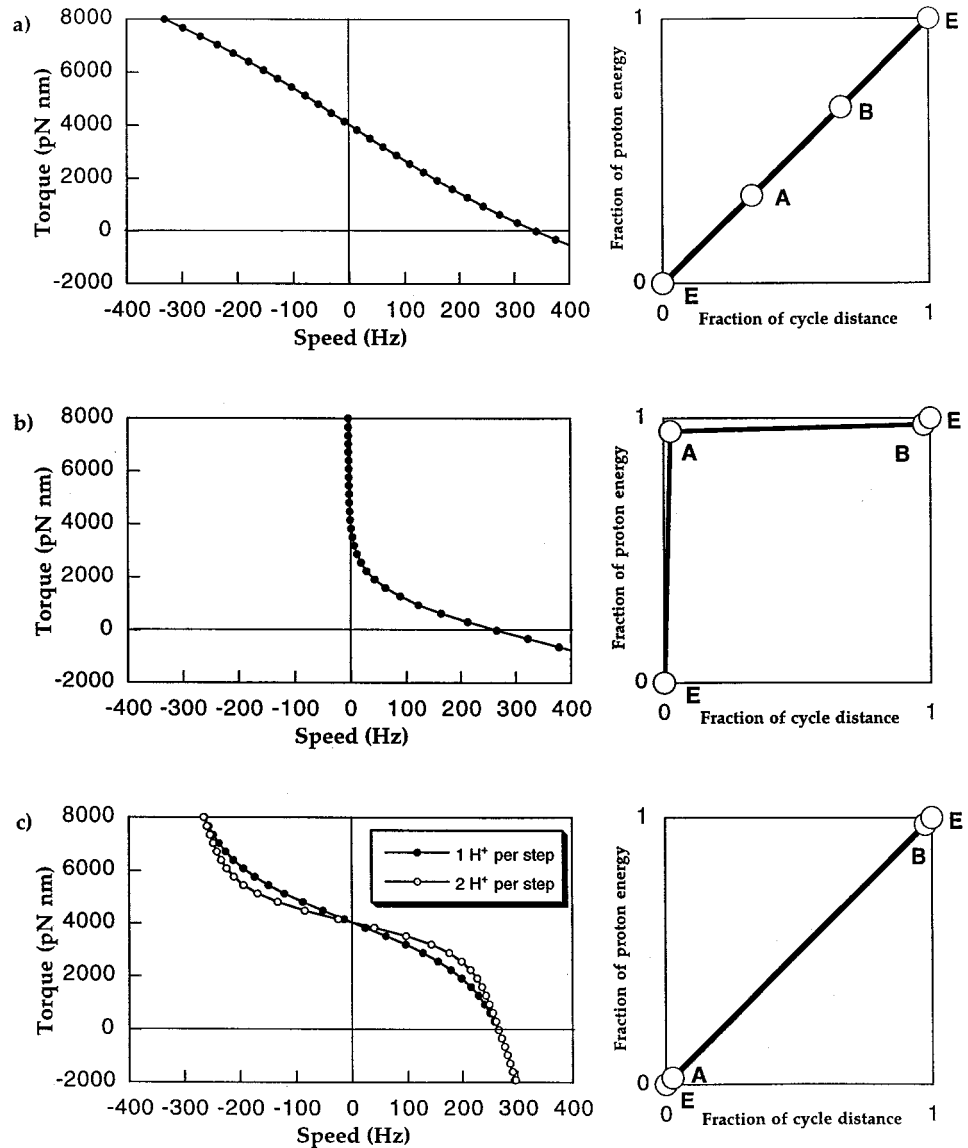
protons. This is a powerstroke mechanism. It could be realized if rotation and proton transit occur simultaneously, as in the half-channel model of Läuger (1988). There is evidence, however, that torque is generated at the interface between the proteins MotA on the stator and FliG on the rotor, on the cytoplasmic side of the membrane (Zhou et al., 1998). For the model of Läuger to be consistent with this evidence, the half-channels would need to be located here and protons would need to arrive at this site with minimal loss of electrochemical potential. Alternatively, the transfer of protons from the periplasm to a cytoplasmic torque-generator would need to utilize the proton free energy to put the torque-generator into a high-energy state. The net forwards rate of step 2 in the model is zero at a torque of 250 pN.nm per unit, where the work and proton free energy terms, W_i and U_i, are balanced. Small changes in torque produce relatively large changes in W_i, upsetting the balance and leading to relatively high speeds in either direction.

Beyond about 300 Hz, step 2 is no longer rate-limiting and the torque-speed curve is determined by the other steps.

The curve marked by filled circles in Fig. 6 *c* shows only a slight torque plateau. To make torque more nearly constant, it is necessary to increase the torque dependence of step 2 further, which can only be done by increasing the distance moved per cycle, ϕ. But this will also have the effect of reducing the torque at which W_i and U_i, are balanced for a given U_i. In order to match the stall torques that have been observed in wild-type flagellar motors, either the number of units per motor must be larger than 8, which is possible, or U_i must be increased beyond the energy available from the transit of a single proton. The curve marked by the open circles in Fig. 6 *c* was obtained by setting $n_s = 60$ for the number of mechanochemical cycles per revolution, assuming that two protons are translocated per cycle and reducing the rate constants, k_i, such that the zero-torque speed remains the same. The same curve could

also be obtained by setting $n_u = 16$ and $n_s = 30$ and halving the new values of k_i.

The experimental results presented here do not determine whether motor torque is constant over the range of speeds studied, or whether it falls linearly with increasing speed. Earlier experiments addressed this question by destroying motor function by ultraviolet irradiation, chemical uncoupling of pmf, or mechanical breakage (Washizu et al., 1993; Berg and Turner, 1993). Subsequent curves of speed versus electrorotation strength were typically parallel to those obtained before the motor was disrupted (at speeds below a few hundred Hz). Under the simplest assumption, the motor exerts negligible drag in its disrupted state and therefore the motor generates constant torque when undamaged. This assumption is reasonable if we assume that the disruption is so great that the damaged motor can only exert passive viscous drag, which can be shown to be negligible for an object with the dimensions of the flagellar motor in a lipid membrane (Berg, 1974). Samuel and Berg (1995) observed rotational diffusion in tethered cells with broken motors and the calculated diffusion coefficients were of the same magnitude as those predicted for a freely rotating object the size of a tethered cell. This assumption also neatly explains the observation that the damaged curves were typically parallel to the intact curves; that is, it is simpler to assume that the damaged motor exerts no drag than it is to assume that it should always exert just enough drag to make the intact and broken curves parallel. However, simple does not necessarily mean true. The possibility remains that the rotor and stator continue to interact in the disrupted state, and that only the means of coupling the torque-generating cycle to the energizing pmf is destroyed. In this case broken motors could exert a considerable and well-defined drag, and the data would indicate that motor torque is not constant over this range of speeds, but decreases linearly with speed.

Assuming tight coupling between proton flux and rotation and a well defined kinetic cycle involving the transit of a fixed number of protons per cycle, the absence of a barrier to backward rotation and the existence of a region of constant or nearly constant torque in the torque-speed curve of the flagellar motor tell us two things. Firstly, the mechanism is likely to be of the powerstroke rather than the thermal ratchet type; any steps that dissipate a significant fraction of the pmf must also involve rotation of the motor or must have reverse rates that do not become rate-limiting even at speeds of 100 Hz backward. Secondly, more than one proton is likely to cross the membrane per mechanochemical cycle of the motor. Alternatively, ion flow and rotation may not be tightly coupled, and the motor may be able to rotate backward without pumping ions against their electrochemical gradient. "Loose-coupled" models (Oosawa and Hayashi, 1986) allow the motor to slip in this way, although models that are in principle loose-coupled can display relatively tight coupling between ion flow and rotation over a wide range of speeds (Berry, 1993). If the motor works as a loose-coupled proton turbine (Berry, 1993; Elston and Oster, 1997), then terms like "powerstroke," "thermal ratchet,"

and "mechanochemical cycle" may be inadequate to describe it. Before these points can be settled, it will be necessary to look in fine detail at the rotation of flagellar motors powered by a single torque generator to see if steps corresponding to single mechanochemical cycles can be observed.

REFERENCES

Berg, H. C. 1974. Dynamic properties of bacterial flagellar motors. *Nature (London).* 249:77–79.

Berg, H. C., and L. Turner. 1993. Torque generated by the flagellar motor of *Escherichia coli. Biophys. J.* 65:2201–2216.

Berry, R. M. 1993. Torque and switching in the bacterial flagellar motor: an electrostatic model. *Biophys. J.* 64:961–973.

Berry, R. M., and H. C. Berg. 1996. Torque generated by the bacterial flagellar motor close to stall. *Biophys. J.* 71:3501–3510.

Berry, R. M., and H. C. Berg. 1997. Absence of a barrier to backward rotation of the bacterial flagellar motor demonstrated with optical tweezers. *Proc. Natl. Acad. Sci. USA.* 94:14433–14437.

Blair, D. F., and H. C. Berg. 1988. Restoration of torque in defective flagellar motors. *Science.* 242:1678–1681.

Block, S. M., and H. C. Berg. 1984. Successive incorporation of force-generating units in the bacterial rotary motor. *Nature.* 309:470–473.

Coppin, C. M., D. W. Pierce, L. Hsu, and R. D. Vale. 1997. The load dependence of kinesin's mechanical cycle. *Proc. Natl. Acad. Sci. USA.* 94:8539–8544.

Elston, T. C., and G. Oster. 1997. Protein turbines I: the bacterial flagellar motor. *Biophys. J.* 73:703–721.

Fahrner, K. A. 1995. Studies of bacterial flagellar motors and filaments. Ph.D. Thesis. Harvard University, Cambridge, MA. 115 pp.

Jones, C. J., R. M. Macnab, H. Okino, and S.-I. Aizawa. 1990. Stoichiometric analysis of the flagellar hook-(basal-body) complex of *Salmonella typhimurium. J. Mol. Biol.* 212:377–387.

Khan, S., and R. M. Macnab. 1980. The steady-state counterclockwise/clockwise ratio of bacterial flagellar motors is regulated by protonmotive force. *J. Mol. Biol.* 138:563–597.

Klein, J. K., and P. H. E. Meijer. 1954. Principle of minimum entropy production. *Phys. Rev.* 96:250–255.

Larsen, S. H., R. W. Reader, E. N. Kort, W. Tso, and J. Adler. 1974. Change in direction of flagellar rotation is the basis of the chemotactic response in *Escherichia coli. Nature.* 249:74–77.

Läuger, P. 1988. Torque and rotation rate of the bacterial flagellar motor. *Biophys. J.* 53:53–65.

Lowe, G., M. Meister, and H. C. Berg. 1987. Rapid rotation of flagellar bundles in swimming bacteria. *Nature (London).* 325:637–640.

Macnab, R. M. 1996. Flagella and motility. *In* Escherichia coli and Salmonella: Cellular and Molecular Biology. F. C. Neidhardt, R. Curtiss III, J. L. Ingraham, E. C. C. Lin, K. B. Low, B. Magasanik, W. S. Reznikoff, M. Riley, M. Schaechter, and H. E. Umbarger, editors. American Society for Microbiology, Washington, DC. 123–145.

Magariyama, Y., S. Sugiyama, K. Muramoto, Y. Maekawa, I. Kawagishi, Y. Imae, and S. Kudo. 1994. Very fast flagellar rotation. *Nature (London).* 371:752.

Meister, M., S. R. Caplan, and H. C. Berg. 1989. Dynamics of a tightly coupled mechanism for flagellar rotation. *Biophys. J.* 55:905–914.

Meister, M., G. Lowe, and H. C. Berg. 1987. The proton flux through the bacterial flagellar motor. *Cell.* 49:643–650.

Oosawa, F., and S. Hayashi. 1986. The loose coupling mechanism in molecular machines of living cells. *Adv. Biophys.* 22:151–183.

Samuel, A. D. T., and H. C. Berg. 1995. Fluctuation analysis of rotational speeds of the bacterial flagellar motor. *Proc. Natl. Acad. Sci. USA.* 92:3502–3506.

Samuel, A. D. T., and H. C. Berg. 1996. Torque-generating units of the bacterial flagellar motor step independently. *Biophys. J.* 71:918–923.

Scharf, B. E., K. A. Fahrner, L. Turner, and H. C. Berg. 1998. Control of direction of flagellar rotation in bacterial chemotaxis. *Proc. Natl. Acad. Sci. USA.* 95:201–206.

Silverman, M., and M. Simon. 1974. Flagellar rotation and the mechanism of bacterial motility. *Nature (London).* 249:73–74.

Sosinsky, G. E., N. R. Francis, D. J. DeRosier, J. S. Wall, M. N. Simon, and J. Hainfeld. 1992. Mass determination and estimation of subunit stoichiometry of the bacterial hook-basal body flagellar complex of *Salmonella typhimurium* by scanning transmission electron microscopy. *Proc. Natl. Acad. Sci. USA.* 89:4801–4805.

Washizu, M., Y. Kurahashi, H. Iochi, O. Kurosawa, S.-I. Aizawa, S. Kudo, Y. Magariyama, and H. Hotani. 1993. Dielectrophoretic measurement of bacterial motor characteristics. *IEEE Trans. Ind. Applications.* 29:286–294.

Zhou, J., S. A. Lloyd, and D. F. Blair. 1998. Electrostatic interactions between rotor and stator in the bacterial flagellar motor. *Proc. Natl. Acad. Sci. USA.* 95:6436–6441.